The importance of the temperature gradient for the processes occurring during high-temperature oxidation of the cladding, its mechanical deformation and oxidation of the melt

J. Stuckert

Abstract

Unlike isothermal conditions in some single effect tests, prototypical reactor conditions and the bundle tests simulating them always exhibit both axial and radial temperature gradients. Such gradients are crucial for a number of effects observed in accident conditions at high temperatures. This presentation describes three such effects: (1) Redistribution of oxygen in cladding under steam starvation conditions; (2) Growth of ceramic precipitates in a metal melt during its oxidation; (3) Dependence of cladding deformation on radial temperature gradient.

In the first case, the heat flow from the pellet to the outer surface of the cladding creates a temperature gradient across the outer cladding oxide layer. In areas of steam starvation, this leads to the formation of metal precipitates in the oxide layer already at temperature (at T≳1200 °C), and not only during the cooling stage.

The second case involves the release of molten cladding metal (through the degrading oxide cladding layer) into the interrod space and its oxidation in the steam. Due to the pronounced exothermic oxidation reaction, the temperature at the surface of the resulting molten pool is higher than in its bulk. This drives the formation of ceramic precipitates within the melt already at temperature, leading to its complete transition to the ceramic phase.

The third case concerns the formation of asymmetric cladding ballooning during a design basis accident. Fuel pellets can maintain their geometric shape up to burnups of 30 MWd/kgU, and a gap remains between the pellet and the cladding. Several pellets are displaced from their axisymmetrical arrangement and touch the cladding at a specific point, forming a hot spot there. As a result, the cladding begins to plastically deform at T>600 °C, primarily near this hot spot. As a result, the circumferential strain of the cladding can remain below 40%, significantly lower than in single rod tests with direct current heating of the cladding.

Karlsruhe Institute of Technology

Institute for Applied Materials

The importance of the temperature gradient for the processes occurring during high-temperature oxidation of the cladding, its mechanical deformation and oxidation of the melt

J. Stuckert

Institute for Applied Materials; Program NUSAFE

Outline

(1) Redistribution of oxygen in cladding under steam starvation conditions.

(2) Growth of ceramic precipitates in a metal melt during its oxidation.

(3) Dependence of cladding deformation on radial temperature gradient.

Evolution of outer oxide layer annealed in Ar at T≈1150 °C without radial temperature gradient: gradual diffusion of oxygen into the metal layers with decrease of ZrO_2 and increase of α-Zr(O)

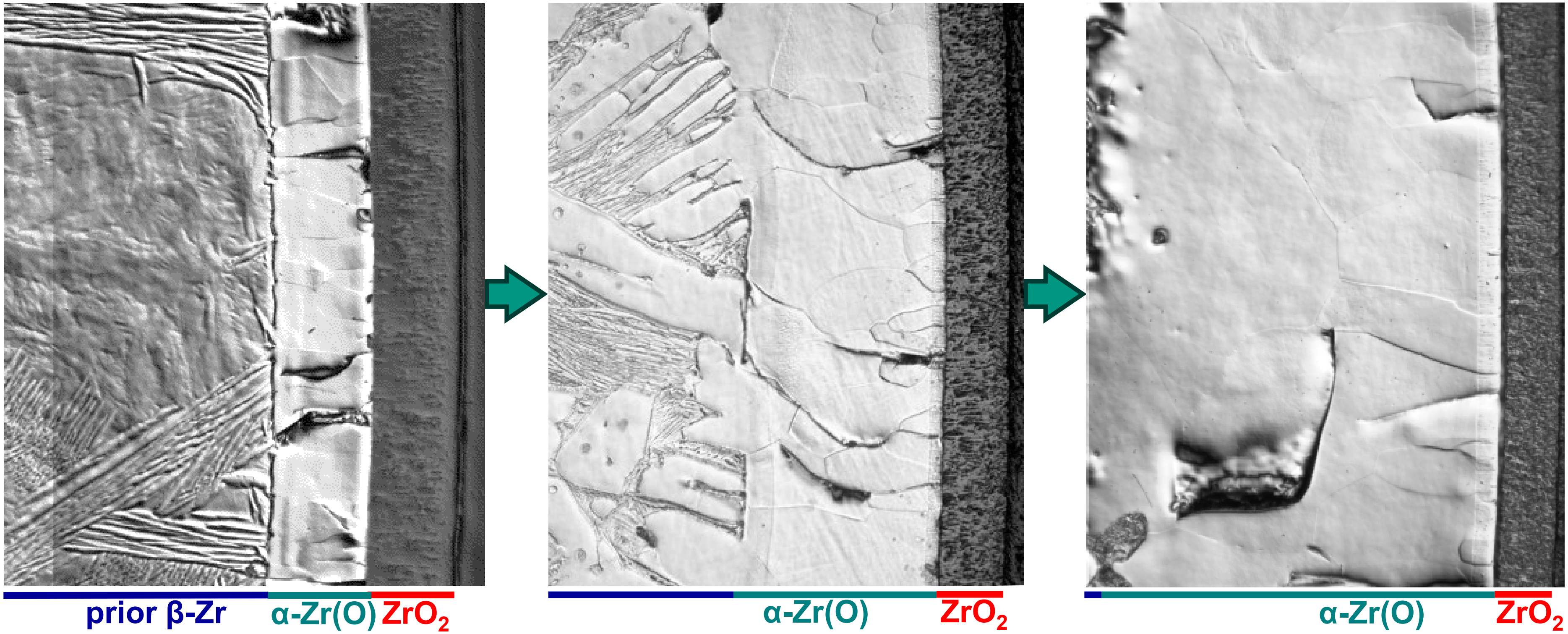

after oxidation in steam:
ZrO_2 73 µm, α-Zr(O) 83 µm,
β-Zr residual

after **annealing** in Ar during 900 s:
ZrO_2 52 µm, α-Zr(O) 165 µm,
β-Zr residual

after **annealing** in Ar during 1800 s:
ZrO_2 43 µm, α-Zr(O) 329 µm,
β-Zr residual

J. Stuckert et al.,
Kinetics of dissolution of oxide layer on cladding surface under oxygen starvation conditions at temperatures between 900°C and 1200°C,
QUENCH-Workshop 20 (2014),
https://www.doi.org/10.13140/RG.2.2.25819.05925

decrease of ZrO_2: $\Delta d_{ox} / t^{1/2} = 287*exp(-8473/T) = 287*exp(-70326/RT)$,

increase of α-Zr(O): $\Delta d_{\alpha} / t^{1/2} = 5*10^6*exp(-19679/T) = 5*10^6*exp(-163611/RT)$,

with $R = 8.314\ J/(mol*K)$

Radial temperature gradient across the cladding oxide layer in single rod and bundle tests (T>1100°C) with flowing steam

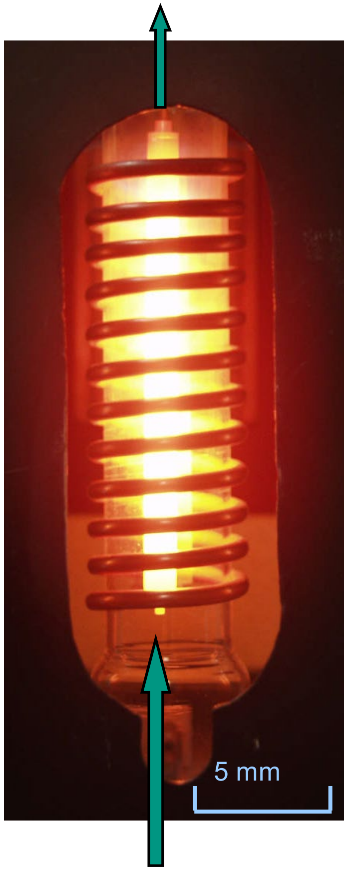

steam, 100 g/h
Ar, 90 l/h

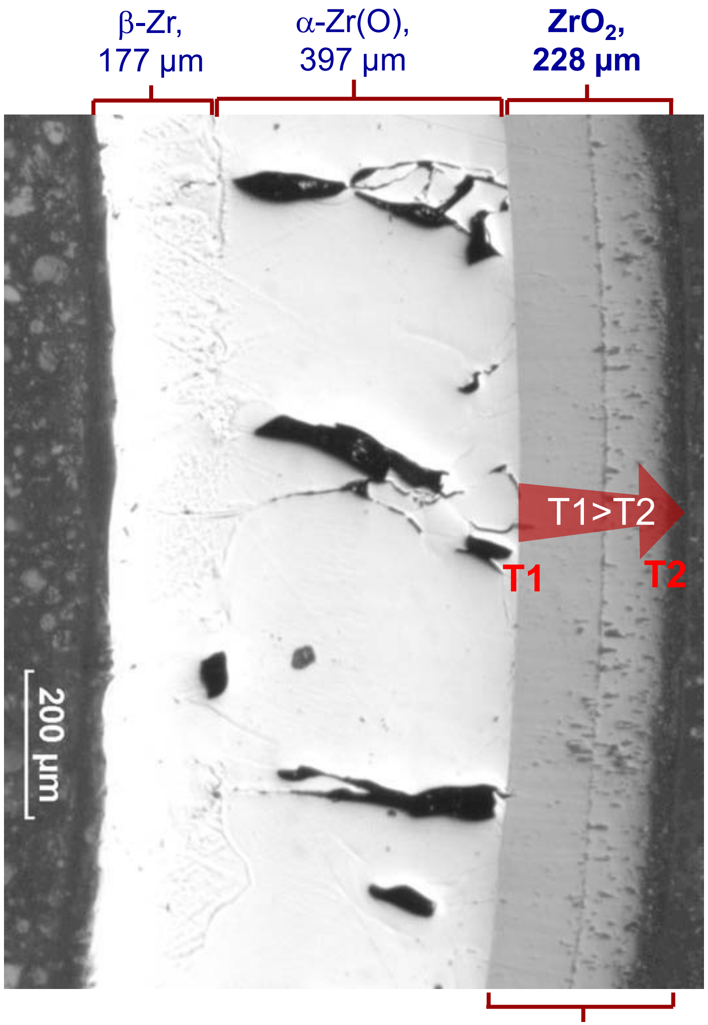

$$|\nabla T| \approx -0.2\ K/\mu m$$

QUENCH-07 bundle:
thick oxide layers
after oxidation in steam

Evolution of outer oxide layer annealed in Ar at T≈1430 °C during 1 h with radial temperature gradient: gradual diffusion of oxygen into the metal layers

reference sample after oxidation in steam during 750 s

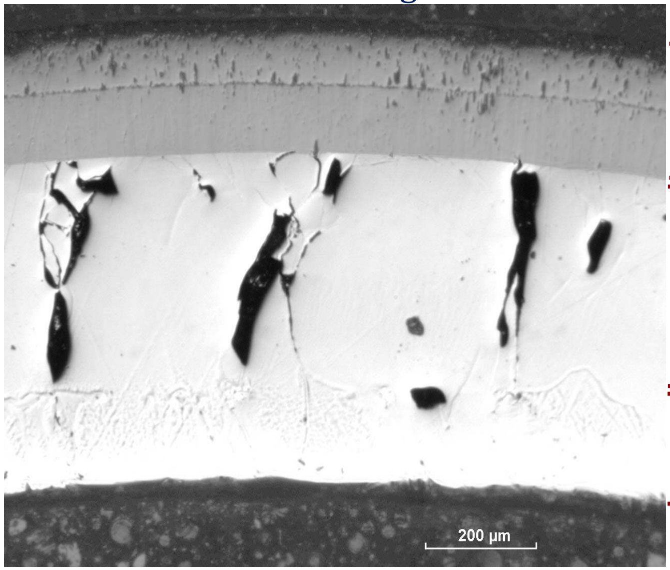

duplex layer ZrO_2, 228 µm

α-Zr(O), 397 µm

β-Zr, 177 µm

test sample after following annealing in Ar during 3 h

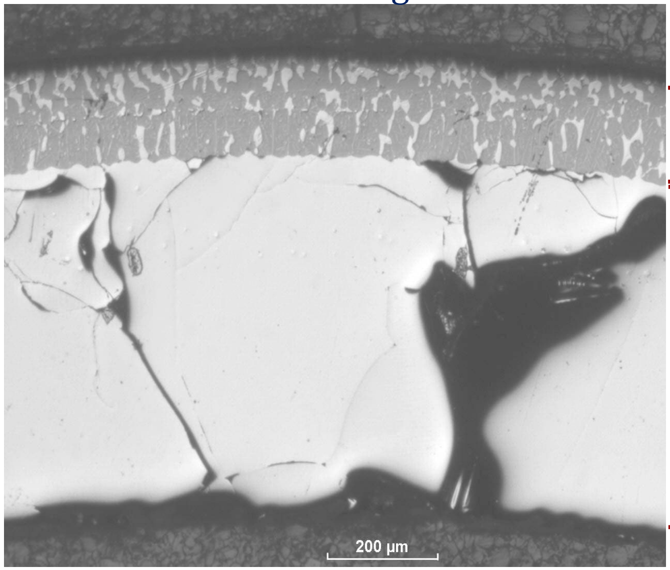

ZrO_2, 186 µm

α-Zr(O), 646 µm

moderate decrease of the ZrO_2 layer thickness;

disappearance of β-Zr layer;

formation of **α-Zr(O) precipitates inside ZrO_2** **at temperature** */it is **not the eutectoid** phase, which can be formed due to decomposition of the sub-stoichiometric ZrO_{2-x} during the cooldown/ ;*

relative large area of precipitates: 24%

J. Stuckert and M. Veshchunov,
Behaviour of Oxide Layer of Zirconium-Based Fuel Rod Cladding under Steam Starvation Conditions,
FZKA-7373 (2008),
https://www.doi.org/10.5445/IR/270071587

A probable explanation for the observed phenomenon is the peculiarity of the phase diagram at the sub-stoichiometric boundary of tetragonal ZrO_2

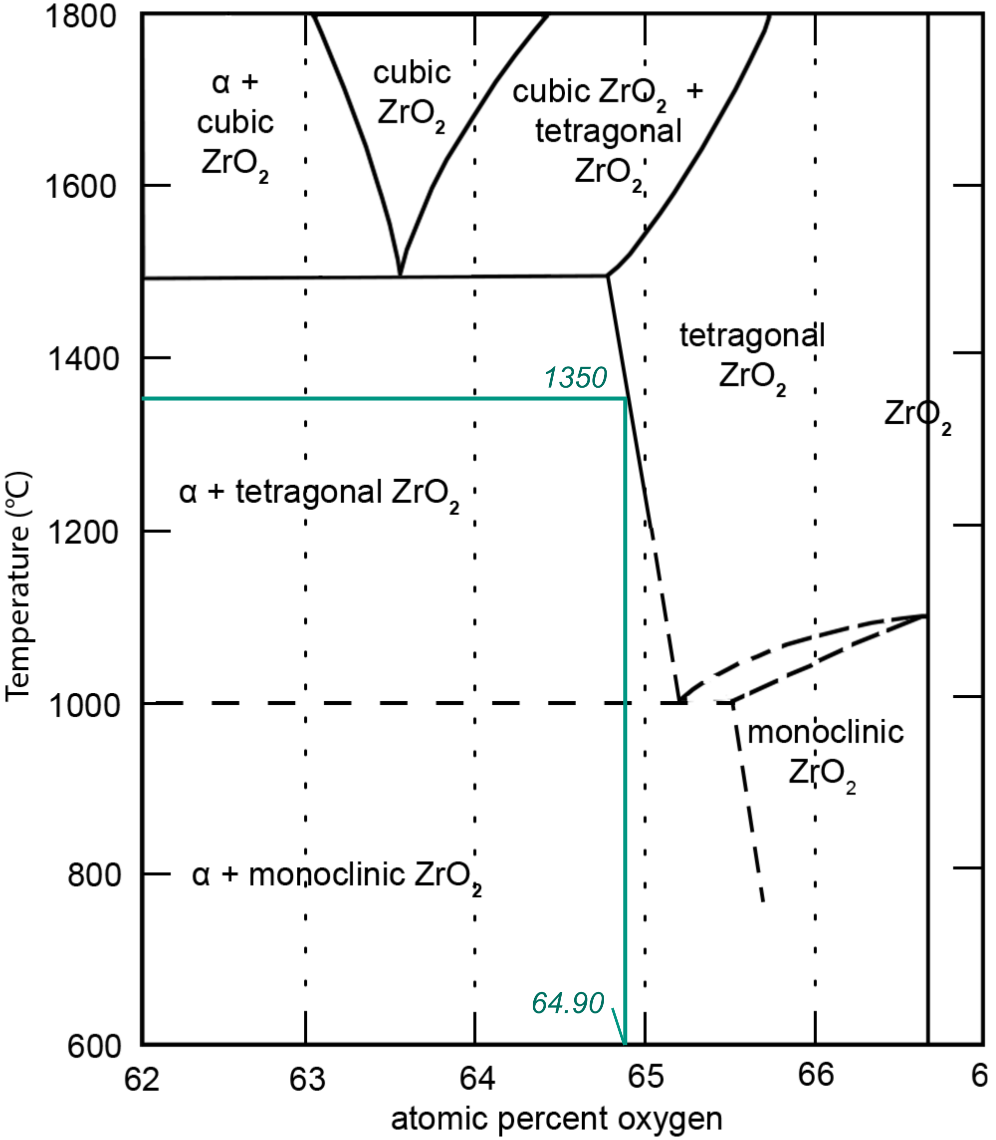

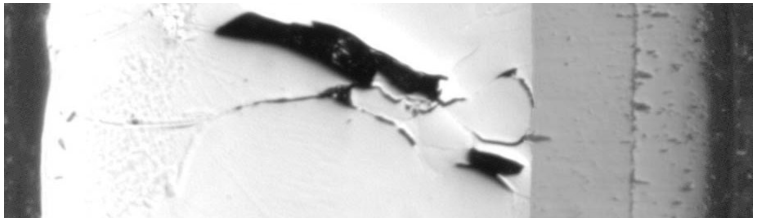

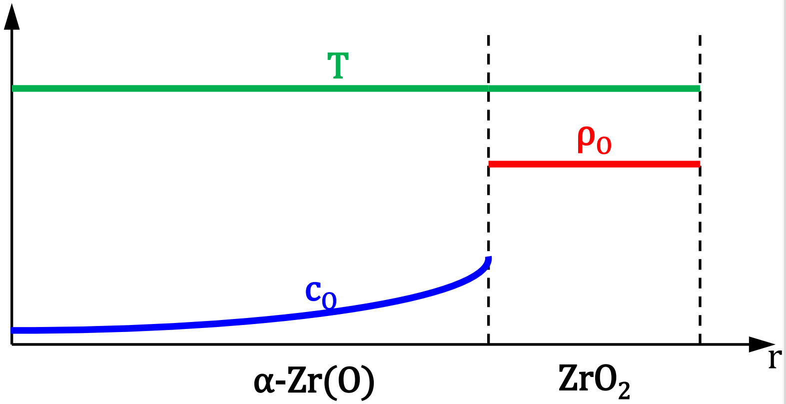

Isothermal conditions

part of Zr-O phase diagram acc. to Domagala and McPherson, Ruh and Garrett

A probable explanation for the observed phenomenon is the peculiarity of the phase diagram at the sub-stoichiometric boundary of tetragonal ZrO_2

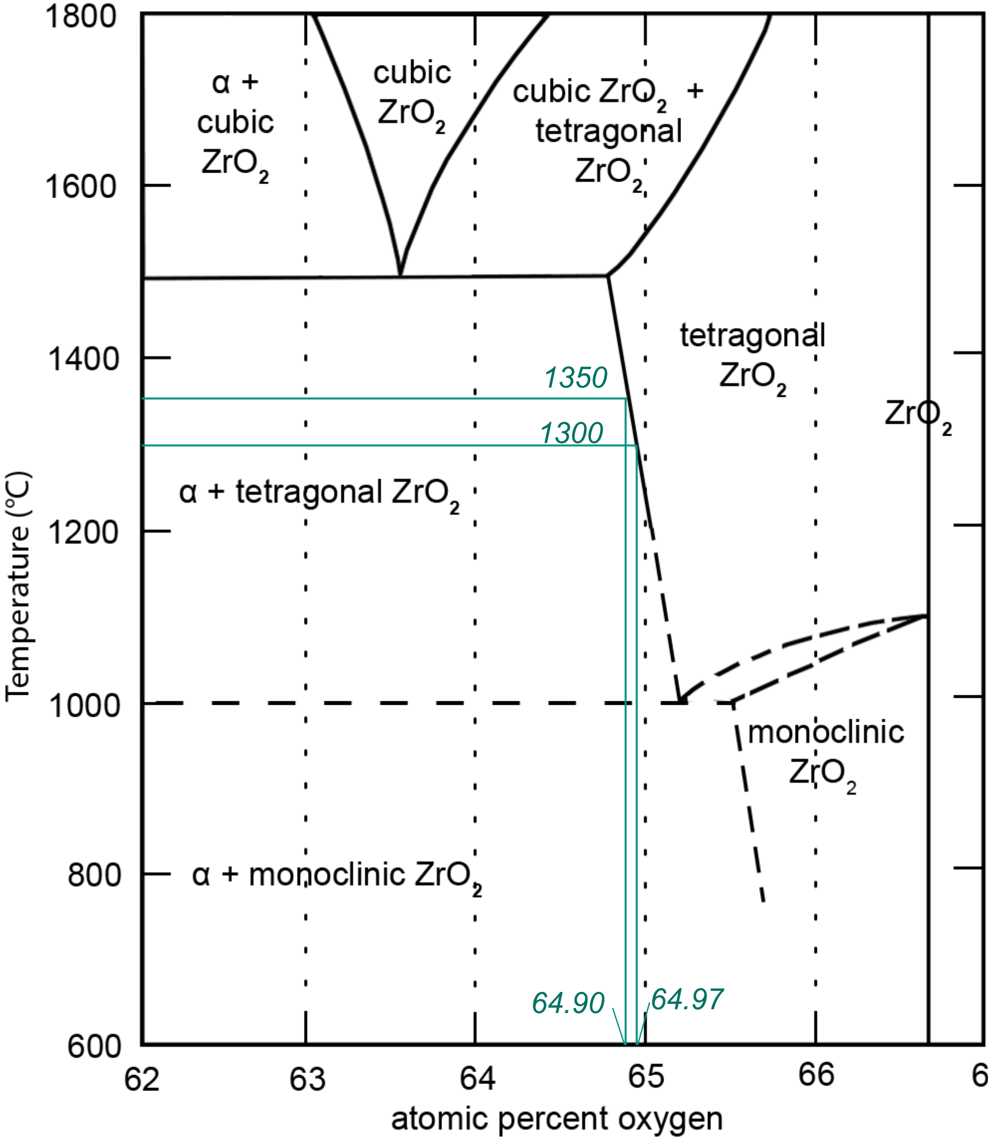

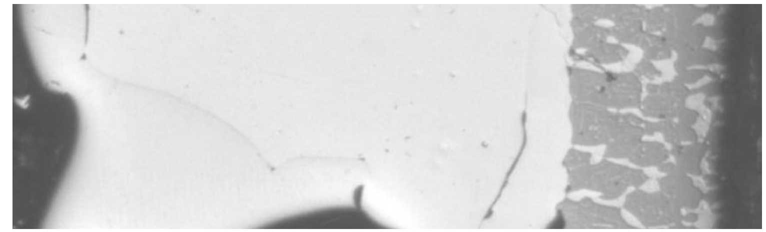

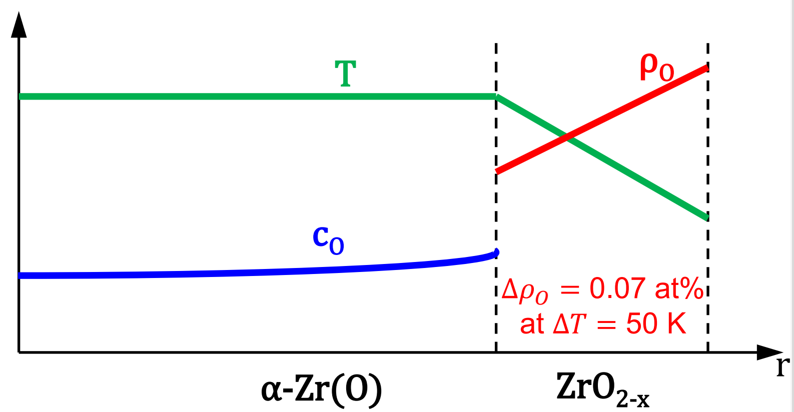

Temperature gradient

↓

Gradient of oxygen concentration

↓

Diffusion of oxygen across the oxide

part of Zr-O phase diagram acc. to Domagala and McPherson, Ruh and Garrett

Experiments at 1300 °C: formation of the outer α-Zr(O) layer after formation of α-Zr(O) precipitates

change of oxide layer after 720 s oxidation during annealing:

- monotonous decrease of the layer thickness
- formation of bulk α-Zr(O) precipitates
- formation of **α-Zr(O) layer** on outer surface of oxide

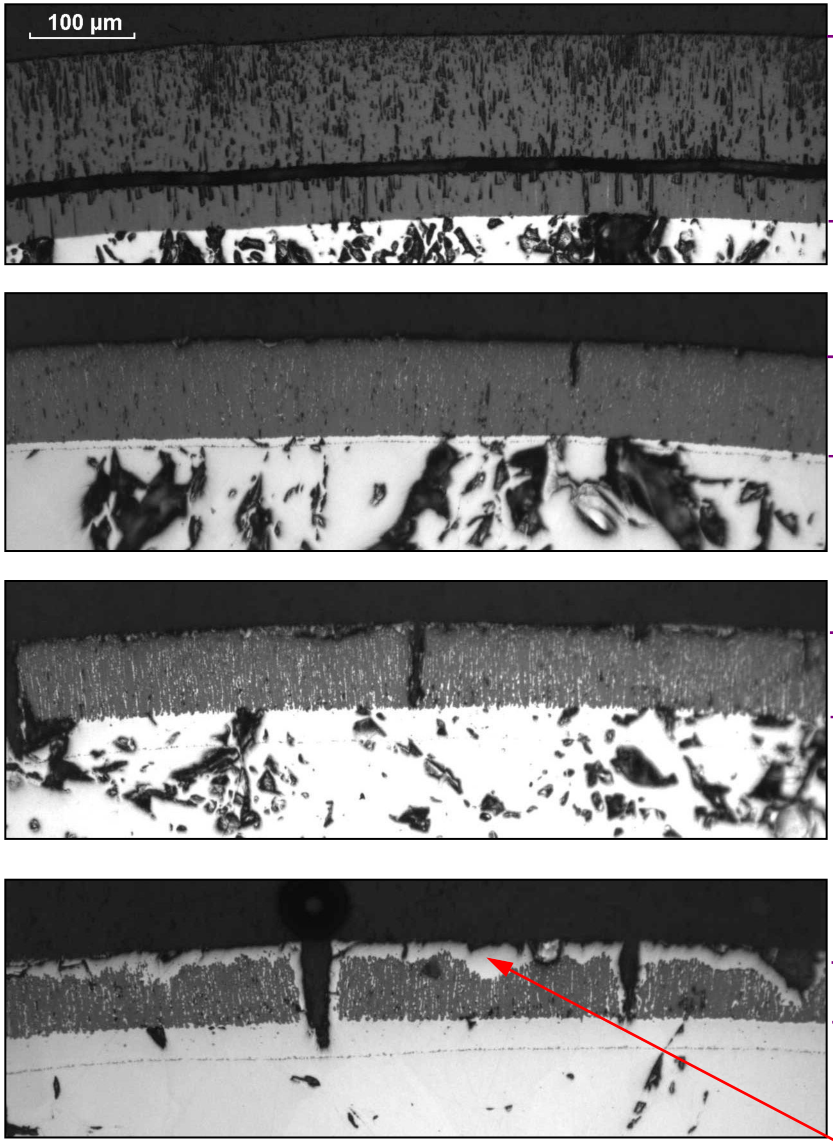

$t_{ann} = 0$ s — 180 µm

$t_{ann} = 2400$ s — 96 µm, precipitates fraction f<15%

$t_{ann} = 5400$ s — 80 µm, precipitates fraction f≈29%

$t_{ann} = 9000$ s — ZrO_{2-x} 55 µm, precipitates fraction f≈29%; outer α-Zr(O) layer δ≈20 µm

Formulas for evaluating numerical quantities

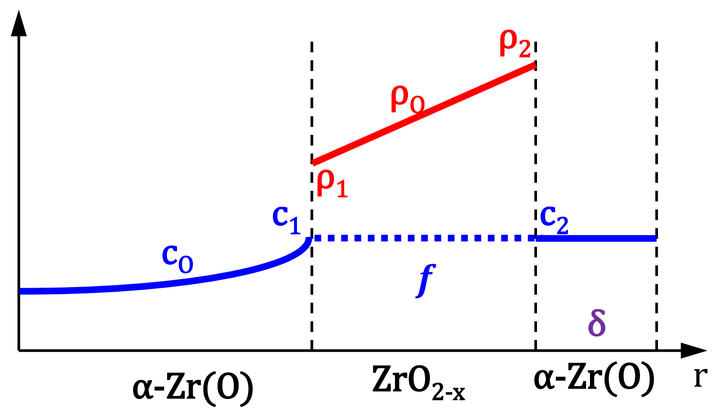

Oxygen concentration profiles in layers of the oxidized cladding after equilibration of ZrO_{2-x} phase under a temperature gradient

According to the Veshchunov's approach:

fraction of α-Zr(O) precipitates in ZrO_2:

$$f \approx \frac{D_O^{ox}}{L_{final}} \cdot \frac{\Delta\rho_O(t)}{L(t)} \cdot \frac{\rho_{Zr}}{c_{Zr}\rho_2 - c_2\rho_{Zr}} \cdot t$$

thickness of outer α-Zr(O) layer formed after cessation of f increase (due to relaxation of compressive stresses):

$$\delta_\alpha^{out} \approx D_O^{ox} \cdot \frac{\Delta\rho_O(t)}{L(t)} \cdot \frac{\rho_{Zr}}{c_{Zr}\rho_2 - c_2\rho_{Zr}} \cdot t$$

where $\rho_{Zr}=35, c_{Zr} = 70, \rho_2=65, c_2=30$;

for tetr. ZrO_2: $D_O^{ox}[\frac{cm^2}{s}] = 8.67 \cdot \exp(-\frac{20380}{T})$,

$D_O^{ox} = 2.05 \cdot 10^3 \mu m^2/s$ @ 1300 °C;

$$\frac{\Delta\rho_O(t)}{L(t)} = const = \frac{0.07}{250} = 2.8 \cdot 10^{-3} \frac{\%}{\mu m} \quad (\text{due to } |\nabla T| \approx 0.2 \frac{K}{\mu m})$$

- The corresponding calculations give values of *f=31%* (after t=5400 s, i.e. L_{final}=80 µm) and δ=*21 µm* (after following t=3600 s), which agrees with the experiment performed at T_{pct}=1300 °C (previous slide)

Influence on air ingress after steam starvation

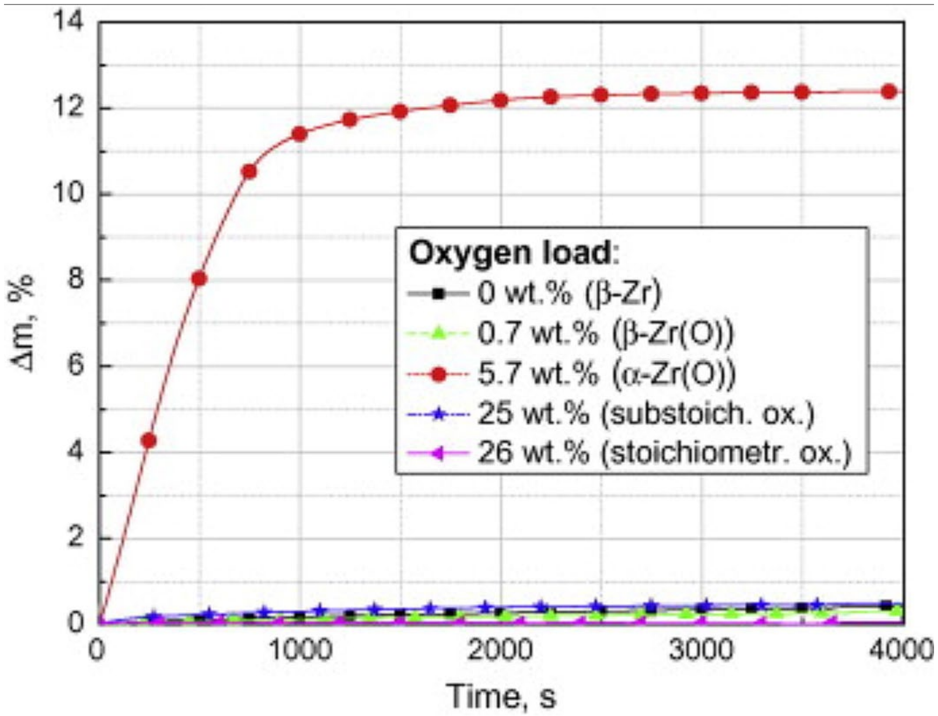

N_2 interaction only with α-Zr(O)

Martin Steinbrück,
High-temperature reaction of oxygen-stabilized α-Zr(O) with nitrogen, JNM 447 (2014), 46-55,
https://doi.org/10.1016/j.jnucmat.2013.12.024

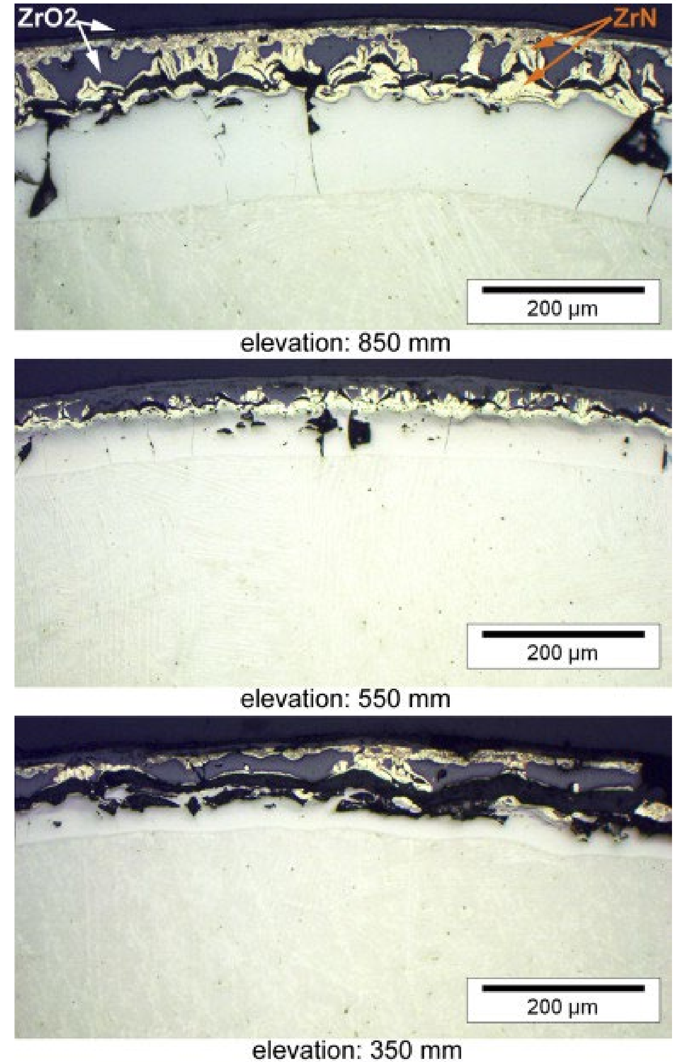

N_2 interaction with α-Zr(O) formed during the steam starvation stage of the QUENCH-16 test

J. Stuckert, M. Steinbrück,
Experimental results of the QUENCH-16 bundle test on air ingress, PNE 71 (2014), 134-141,
https://doi.org/10.1016/j.pnucene.2013.12.001

Sequence of phenomena in the ZrO_2 layer due to oxygen diffusion into the inner metallic layers during steam starvation

- For T ≳ 1400 °C
  - Equilibration of ZrO_{2-x} phase (transition from stoichiometric ZrO_2 to substoichiometric ZrO_{2-x}).
  - Movement of the boundary between ZrO_{2-x} and α-Zr(O) layers, growth of α-Zr(O) precipitates inside the ZrO_{2-x} layer until the internal α-Zr(O) layer is saturated with oxygen.

- For T ≲ 1400 °C
  - Equilibration of ZrO_{2-x} phase.
  - Thickness decrease of the ZrO_{2-x} layer, growth of α-Zr(O) precipitates inside the ZrO_{2-x} layer.
  - Cessation of α-Zr(O) precipitates growth due to relaxation of compressive stresses inside the oxide layer.
  - Growth of the outer α-Zr(O) layer until the internal α-Zr(O) layer is saturated with oxygen.

(2)

Cladding melt release and relocation

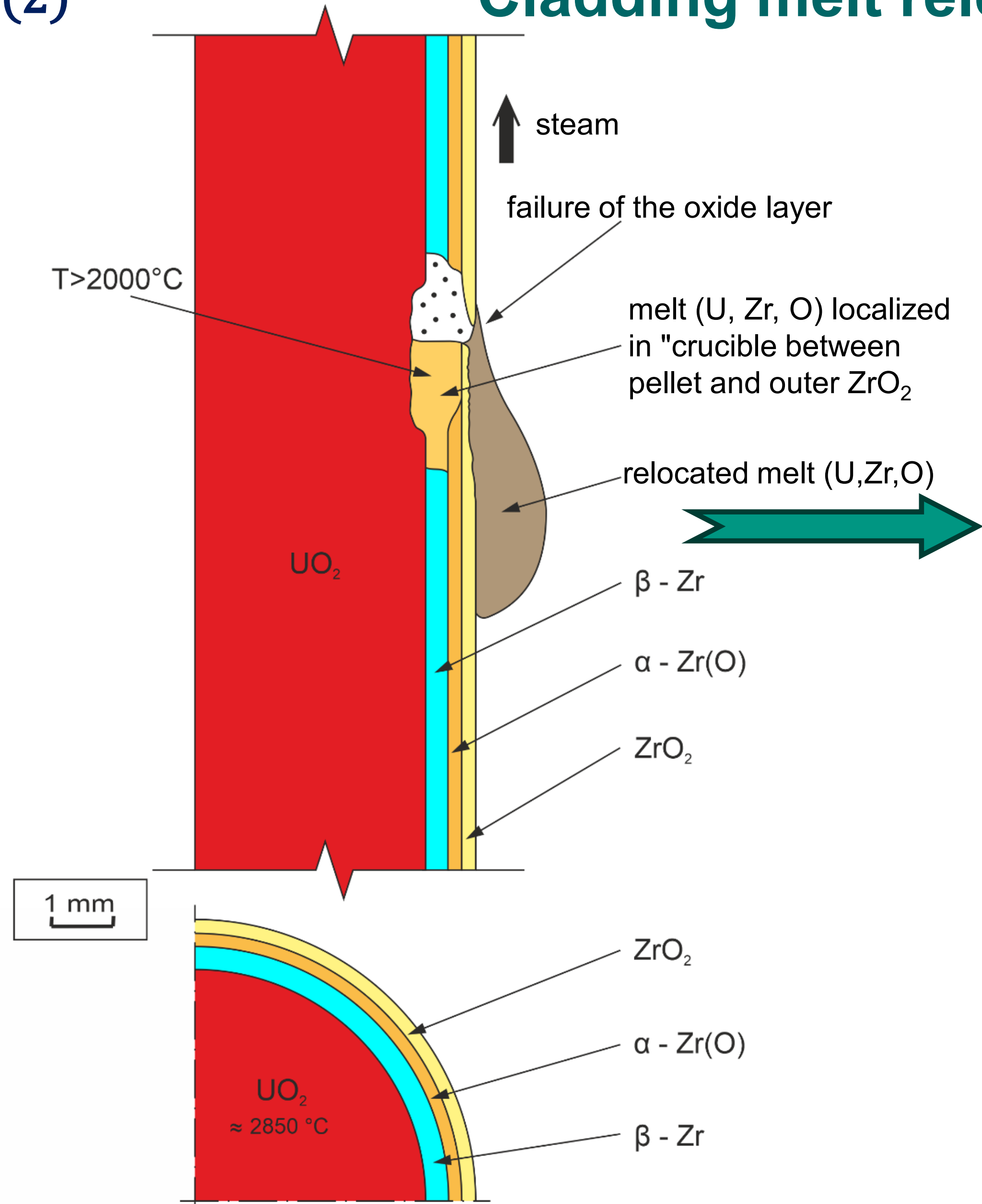

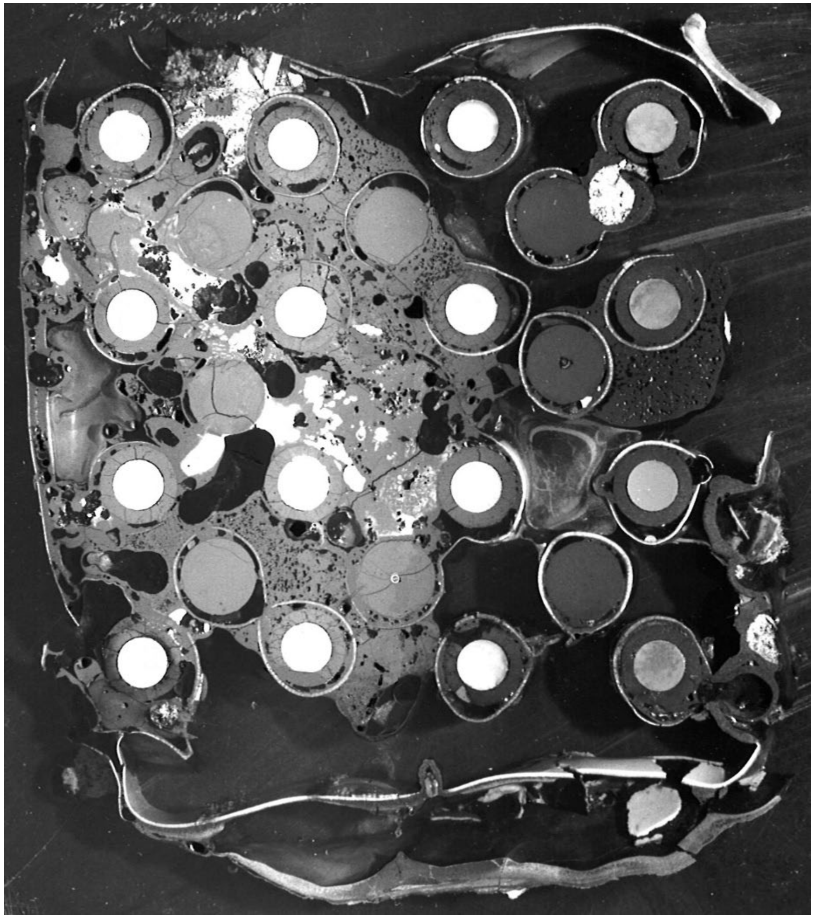

partial blockage of the CORA-05 bundle at the bundle elevation 408 mm with the melt relocated from upper elevations

Structure of frozen melt in molten pools and inside pellet/cladding gap in the QUENCH-02 bundle

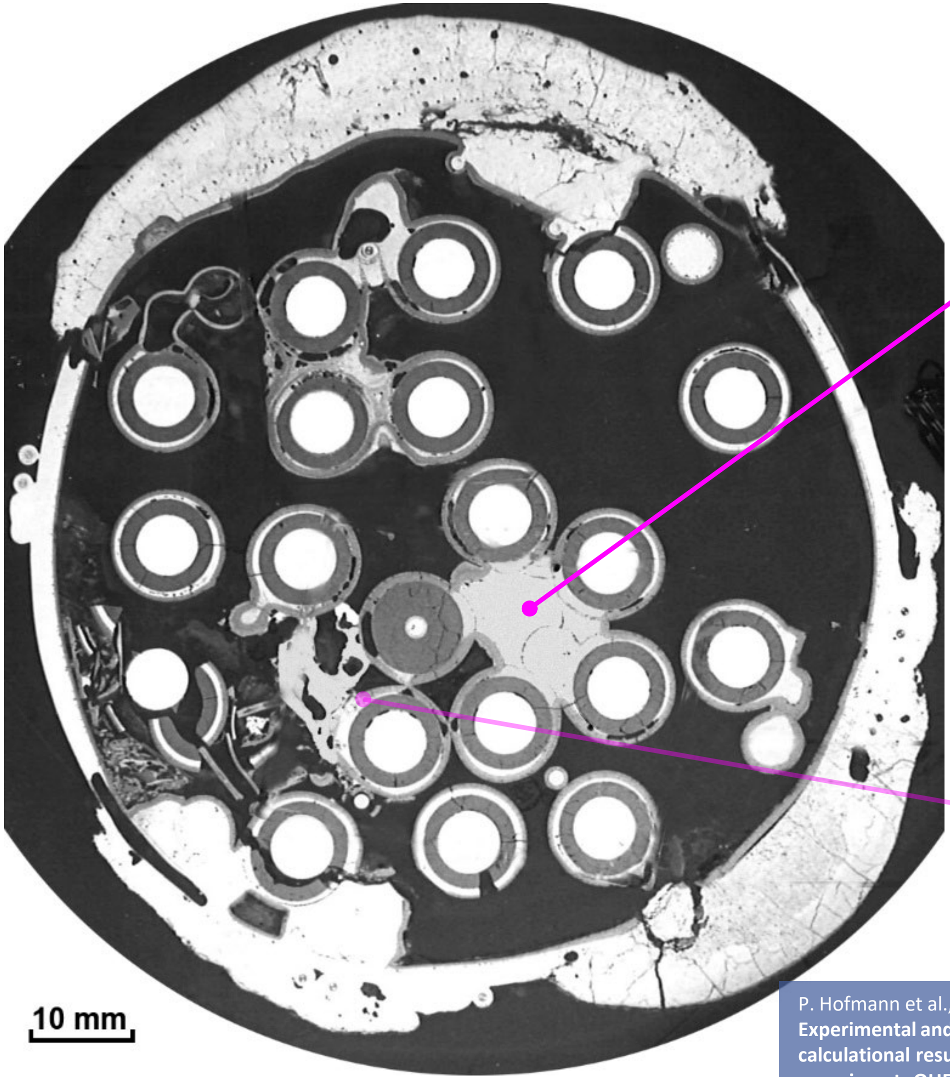

QUENCH-02 bundle, elevation 850 mm

P. Hofmann et al., **Experimental and calculational results of the experiments QUENCH-02 and QUENCH-03**, FZKA-6295 (2000)

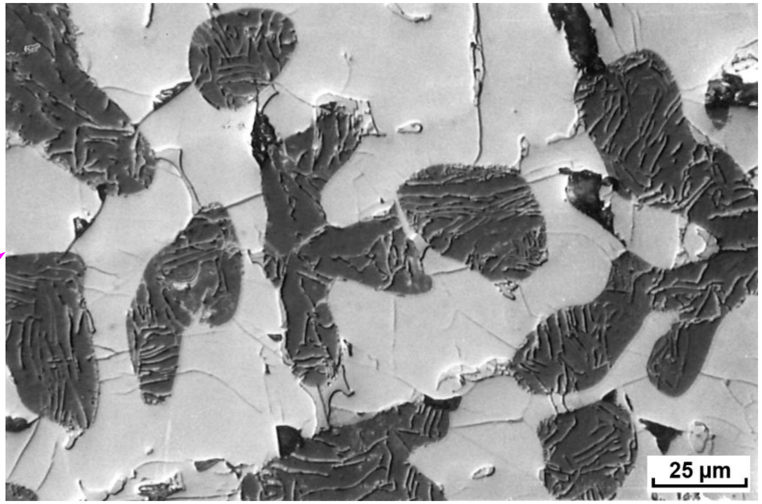

ceramic precipitates in molten pool:
43% area acc. to image analysis

ceramic precipitates in the cladding-pellet gap:
35% area acc. to image analysis

Determination of oxygen content in oxidized Zr melt

Karlsruhe Institute of Technology

Simplified equilibrium Zr-O phase diagram

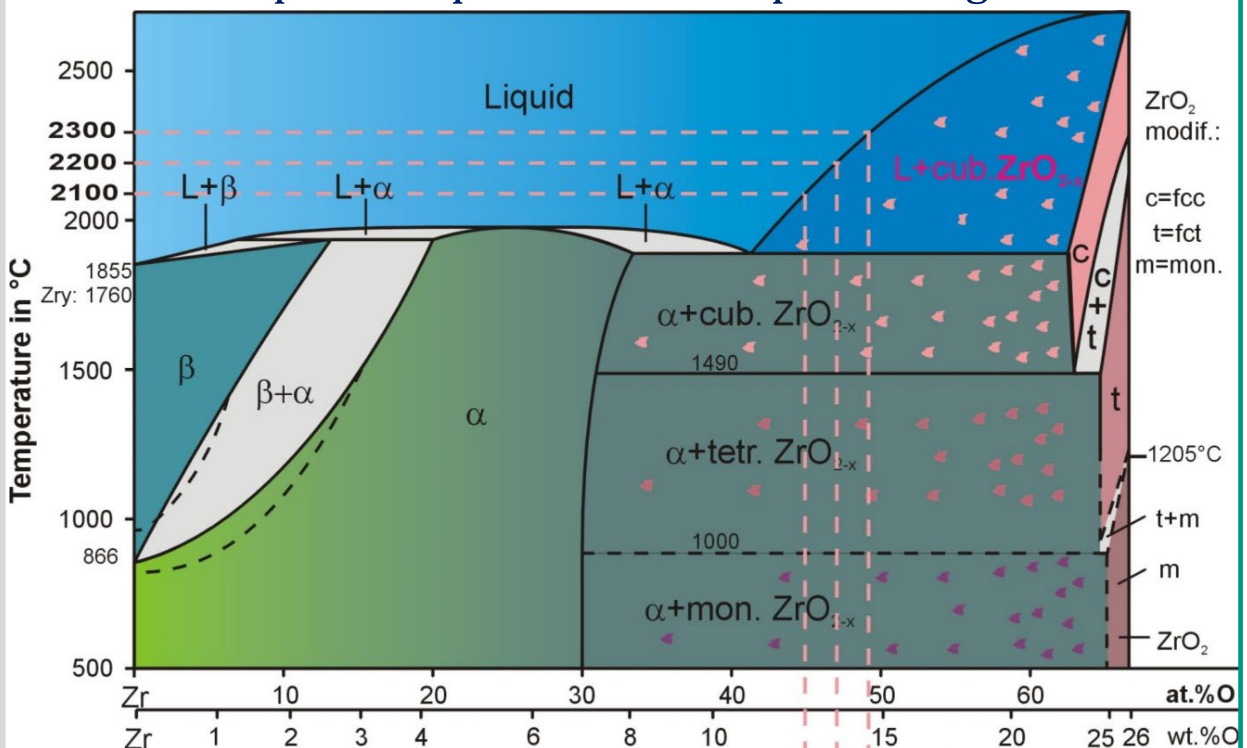

Solubility of oxygen in Zr liquid at 2100, 2200, 2300 °C:

45.3	47	49.5	at.%O
12.7	13.5	14.7	wt.%O

P. Hofmann, J. Stuckert, A. Miassoedov, M. Veshchunov, A. Berdyshev, A. Boldyrev, ZrO_2 dissolution by molten zircaloy and cladding oxide shell failure. New experimental results and modelling, FZKA-6383 (1999), https://doi.org/10.5445/IR/270046616

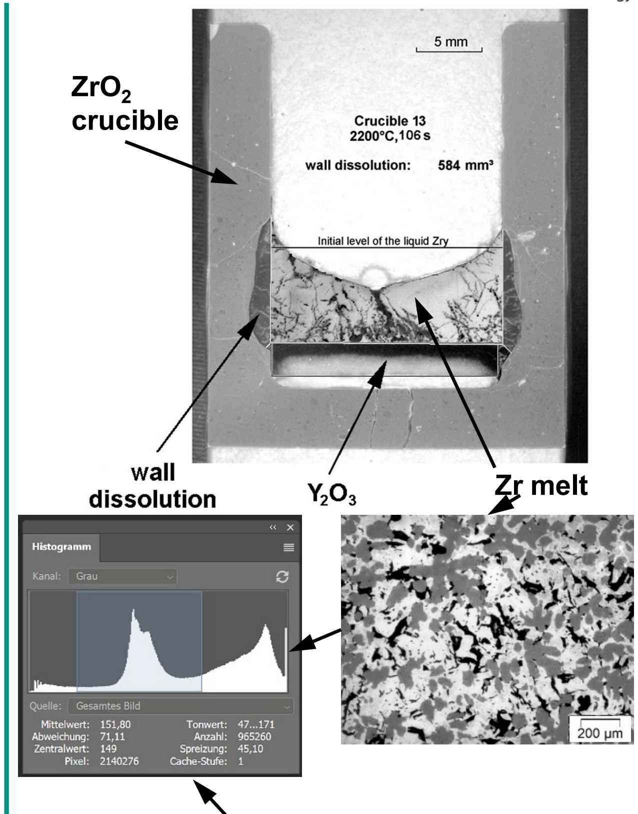

From the image analysis of the ceramic phase content in crucible tests with known relationship between dissolved ZrO_2 and the resulting amount of ceramic precipitated in the solidified melt, the following formula was derived:

$$O = 0.186 \cdot (A+34)$$

where O is in weight %, A – in area %.

IAM Institute for Applied Materials

Structure of frozen melt formed as molten pool in the QUENCH-16 bundle

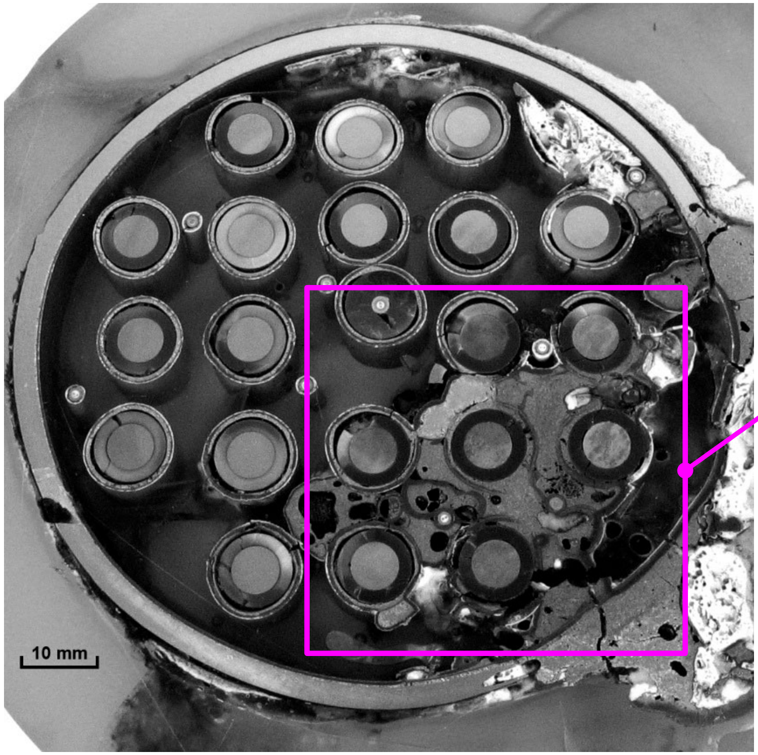

QUENCH-16, elevation 450 mm

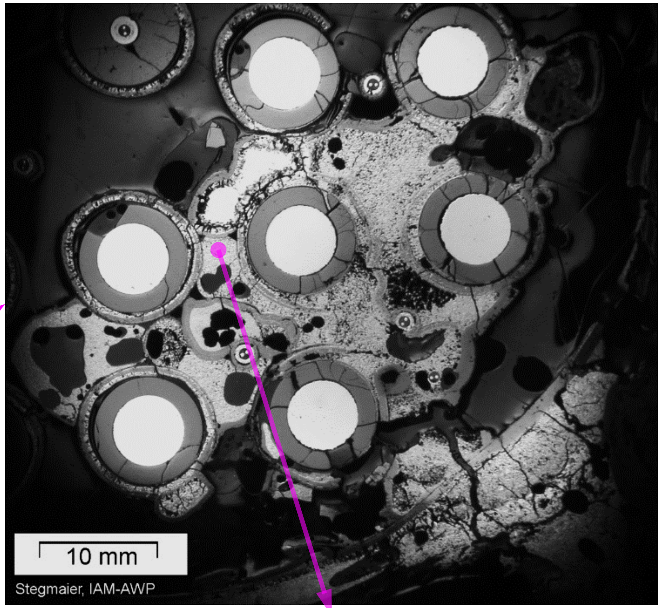

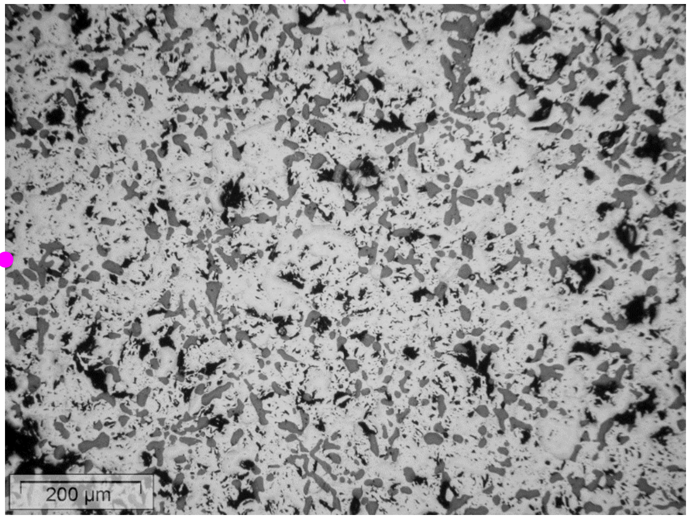

J. Stuckert, M. Steinbrück, **Experimental results of the QUENCH-16 bundle test on air ingress**, PNE 71 (2014), 134-141

area of ceramic precipitates 23% ⇨ 10.6 wt% of O,

this is <u>below</u> the solubility limit (12.7 wt% at 2100 °C)

Structure of frozen melt formed as molten pool in the QUENCH-11 bundle

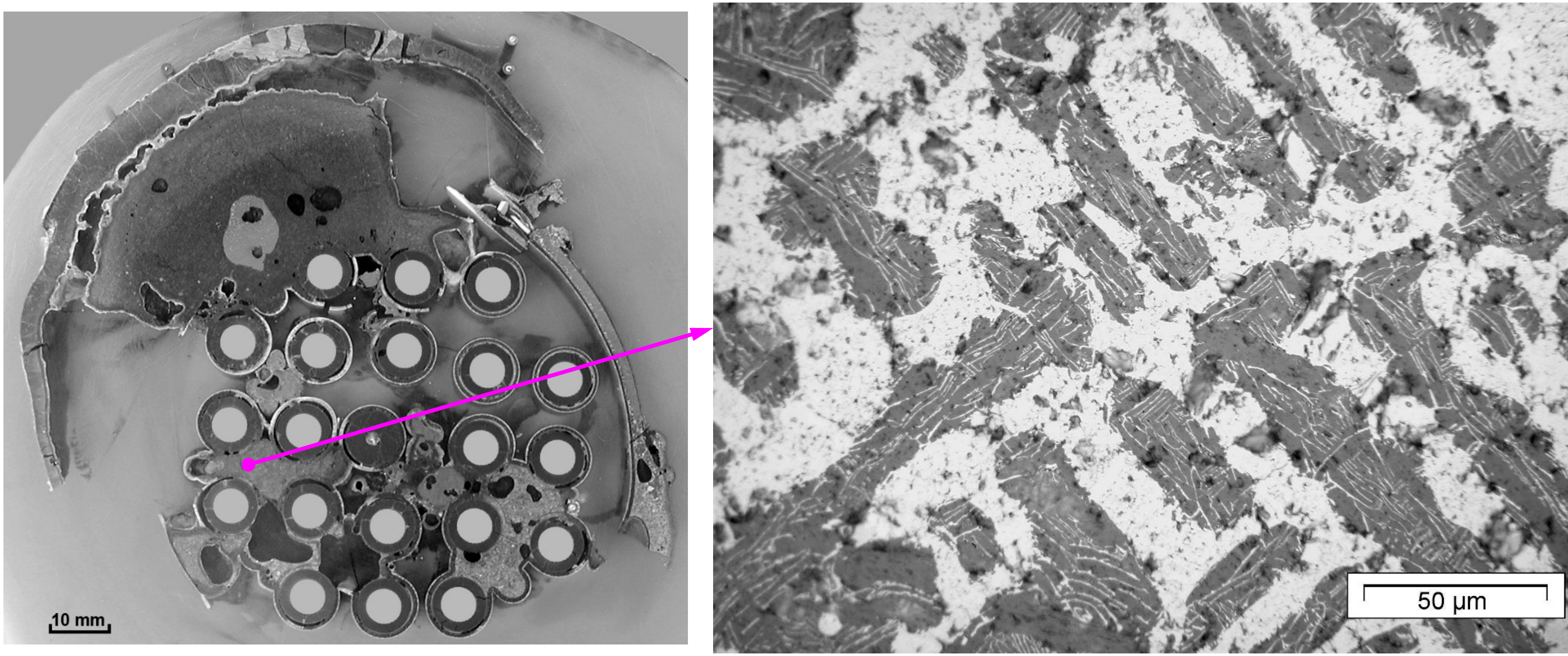

QUENCH-11 bundle test, elevation 850 mm

area of ceramic precipitates 56% ⇨ 16.7 wt% of O,

this is <u>above</u> the oxygen solubility limit

(14.7 wt% at 2100 °C)

Oxygen diffusion to the saturated melt due to T gradient

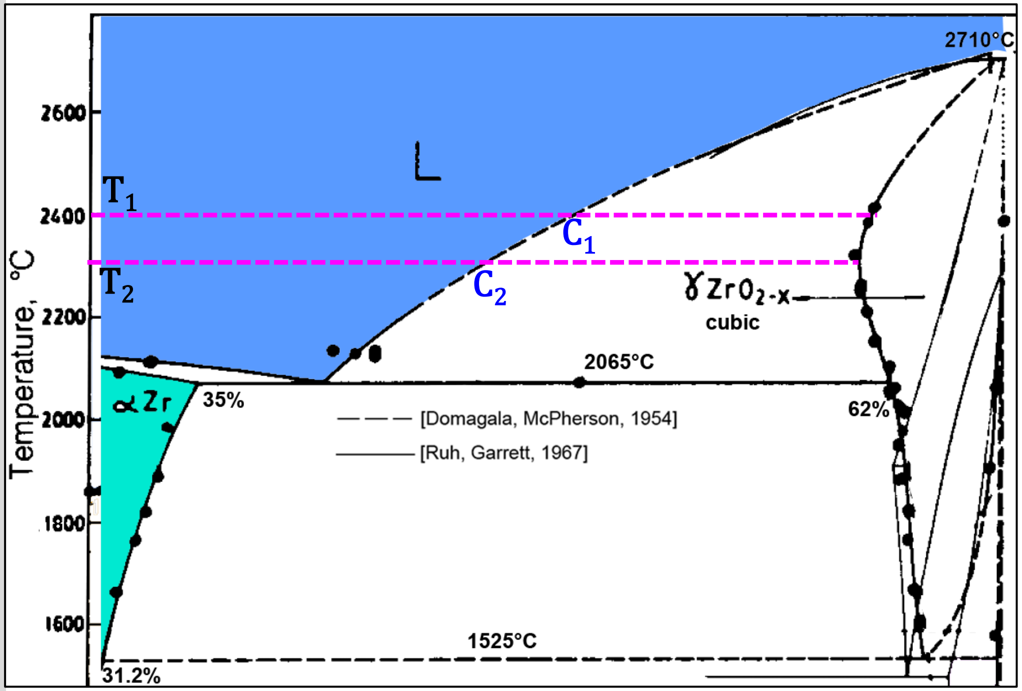

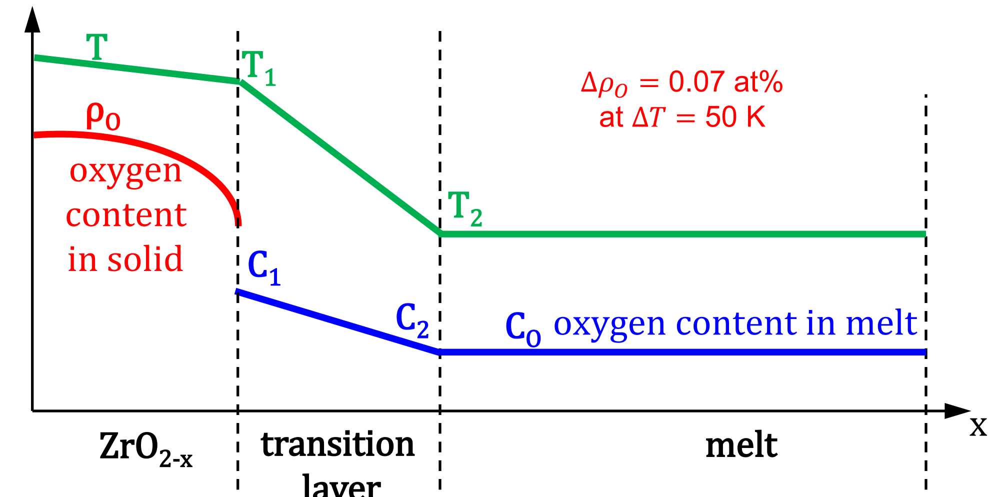

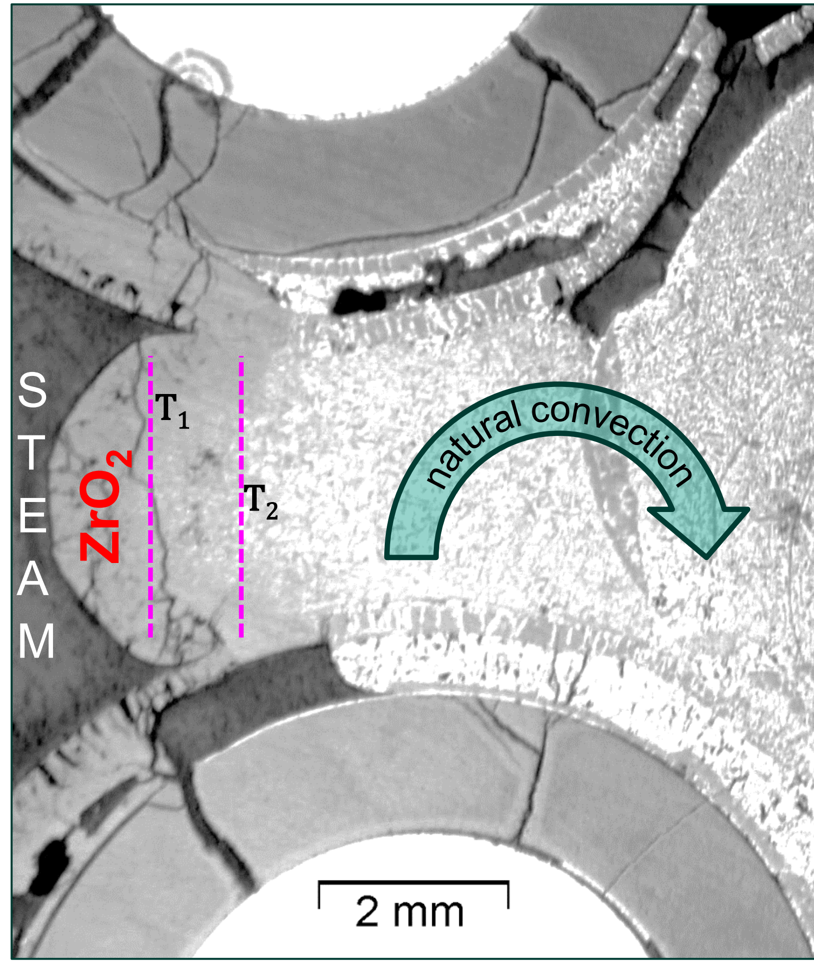

$T_1 > T_2$ due to exothermic reaction of steam with molten Zr

M. Veshchunov, J. Stuckert, A. Berdyshev, Modelling of Zr-O and U-Zr-O melts oxidation and new crucible tests, FZKA-6792 (2002), https://doi.org/10.5445/IR/270046616

Structure of frozen melt formed in the CORA-W2 bundle <u>at temperature</u> and during cooldown

Karlsruhe Institute of Technology

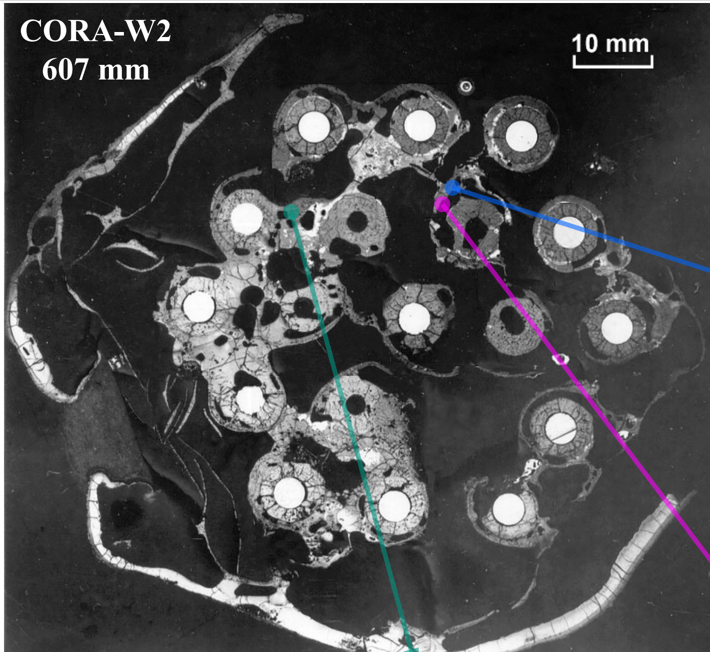

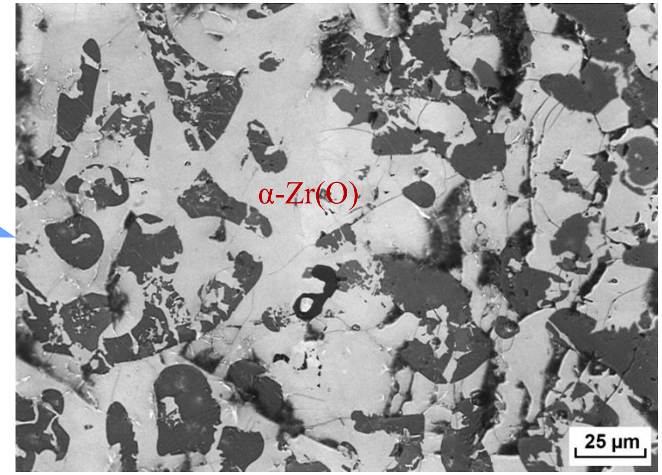

ceramic precipitates 34% → melt <u>saturated</u> with oxygen

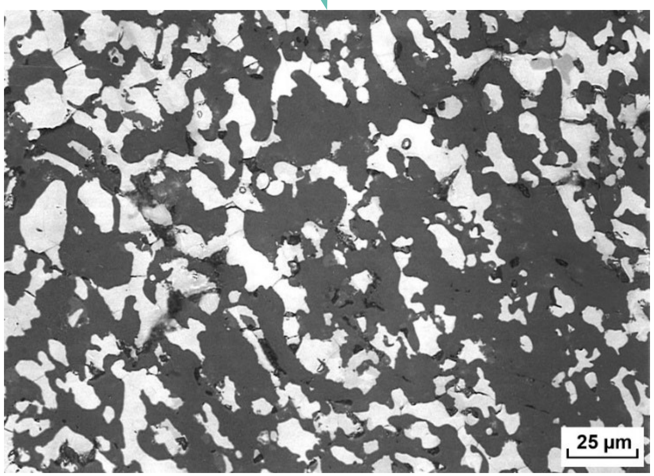

ceramic precipitates 56% → <u>oversaturated</u> melt

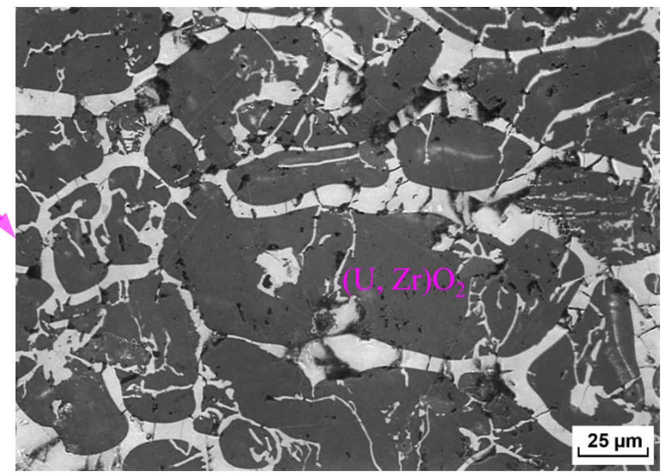

ceramic precipitates 68% → <u>oversaturated</u> melt

According to the EDX analysis of the oxidized melt, the zirconium content in it (in at%) is 4-8 times higher than the uranium (which entered the melt due to the dissolution of the pellets). Therefore, the presence of zirconium is the determining factor.

Oxygen uptake by molten pools at 2200 °C: comparison of two models (SVECHA mechanistical model vs. engineering approach)

Karlsruhe Institute of Technology

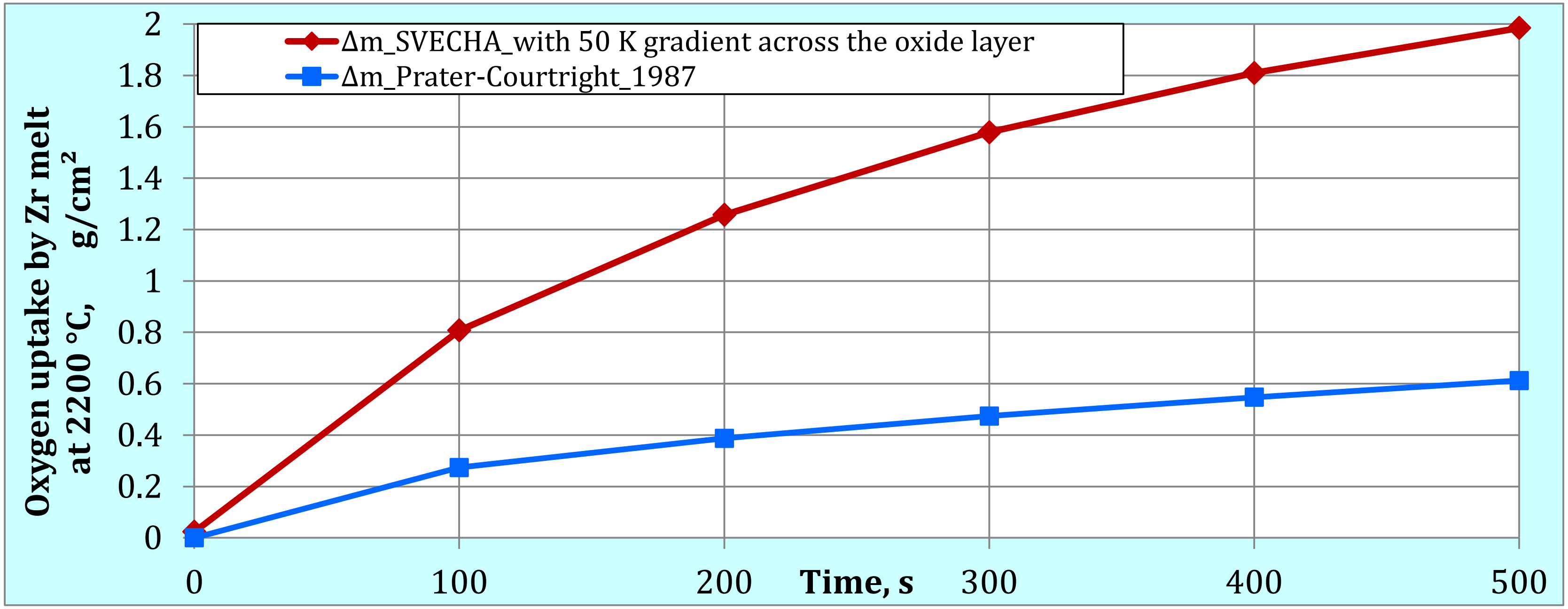

t, s	mass gain by ZrO_2 layer $\Delta m_{R\text{-}r}$, g/cm^2	mass gain by ZrO_2 precipitates in melt m_f, g/cm^2	total mass gain Δm_{SVECHA}, g/cm^2	*Prater-Courtright mass gain Δm_{PC}, g/cm^2*	$\Delta m_{SVECHA}/\Delta m_{PC}$
0	0.023	0	**0.023**	0	
100	0.057	0.751	**0.807**	0.274	3.0
200	0.088	1.169	**1.257**	0.387	3.2
300	0.120	1.458	**1.578**	0.474	3.3
400	0.153	1.657	**1.809**	0.547	3.3
500	0.182	1.803	**1.984**	0.612	3.2

- **accelerated melt oxidation due to formation of ceramic precipitates: factor 3 in comparison to the Prater-Courtright**
- **suggested kinetics:** $K_{mod}=5.74 \cdot exp(-85900/RT)$, $g/cm^2/s^{0.5}$ *(instead $K_{PC}=5.74 \cdot exp(-109911/RT)$, $g/cm^2/s^{0.5}$)*

Phenomena occurring in an oxidizing melt

- The analysis of the viscous melt behavior in bundles and the image analysis of the frozen melt show the formation of ceramic precipitates in the melt even in the molten state (not only during the cooldown).
- The driving mechanism for the formation of melt oversaturated with oxygen and precipitation of ceramic phase is the temperature gradient at the oxide-melt interface of the molten pool.
- According to the Zr-O phase diagram, this ensures a decreasing oxygen concentration in the transition layer and therefore diffusion of oxygen from the oxide to the saturated melt , which is then mixed as a result of natural convection.
- A numerical calculation carried out for the case with an operating temperature of 2200 °C and a temperature gradient at the melt boundary of 50 K showed that the oxidation process occurs parabolically and *three times faster* than predicted by the Prater-Courtright oxidation correlation used usually in computer codes at $T \gtrsim 1800$ °C.

Dependence of the circumferential temperature difference on the position of **contact** between the pellet and the cladding

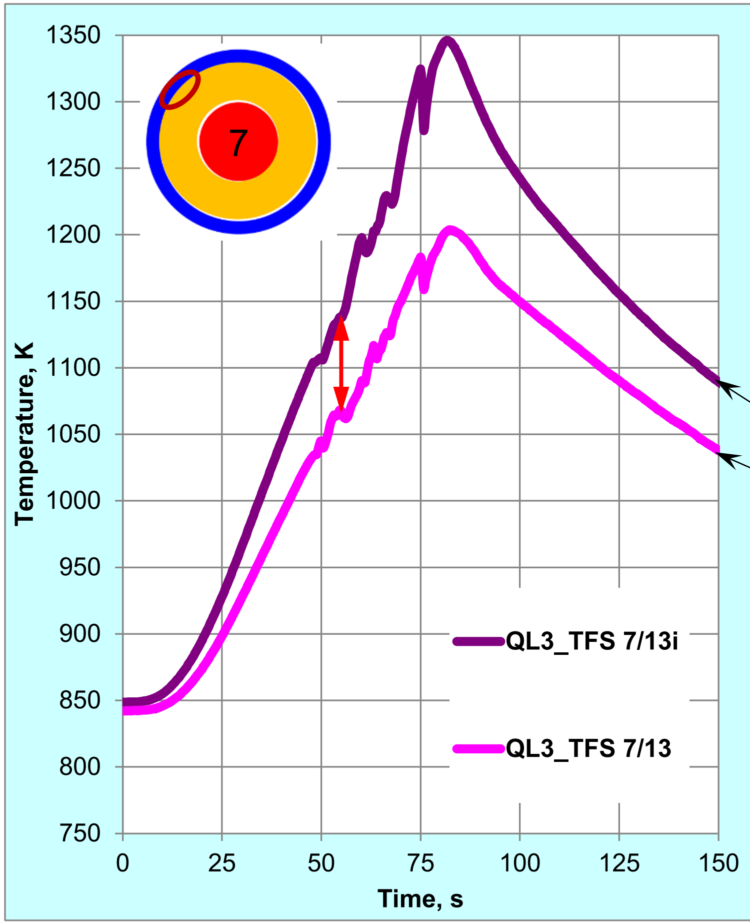

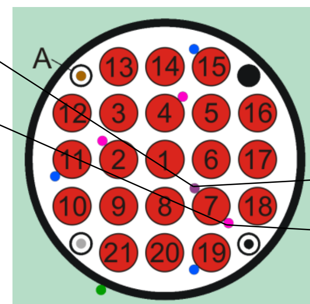

positions of two diametrically opposite TCs on the surface of the rod 7

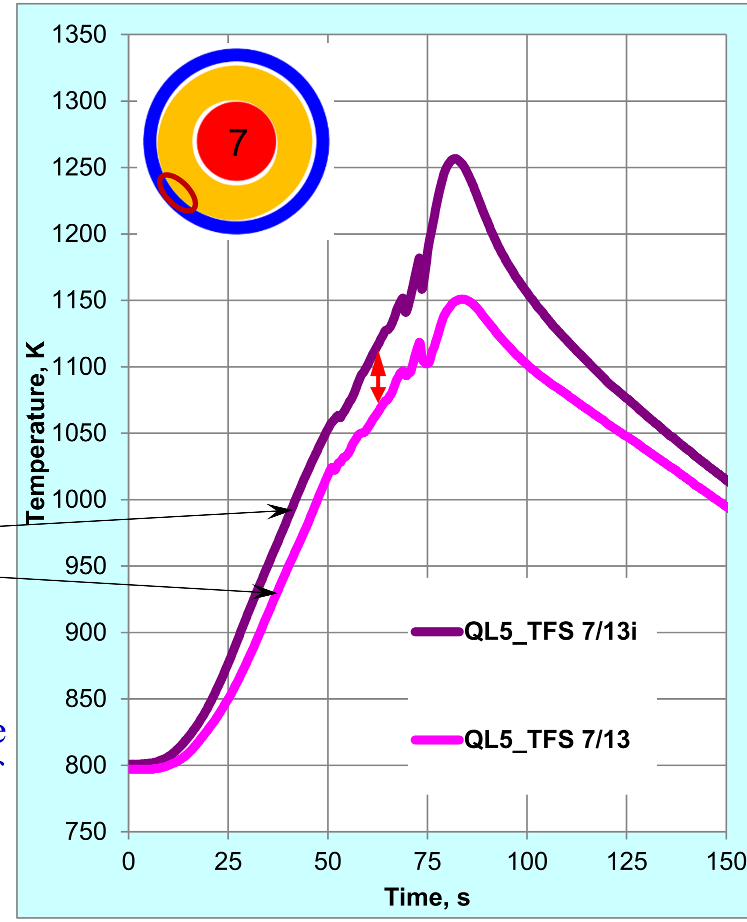

QL-3 bundle:
large circumferential difference ΔT=70 K

QL-5 bundle:
moderate circumferential gradient ΔT=50 K

Not symmetrical cladding ballooning due to point contact between pellet and cladding (QL4 bundle, rod 1, tomography of rod between 903 and 920 mm)

optical view of clad inner surface below the burst opening at 920 mm

hot spot: pellet-cladding contact

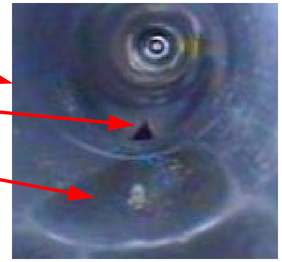

the gap is present until burnouts of 30 MWd/kgU

max gap 150 µm

not changed during ballooning

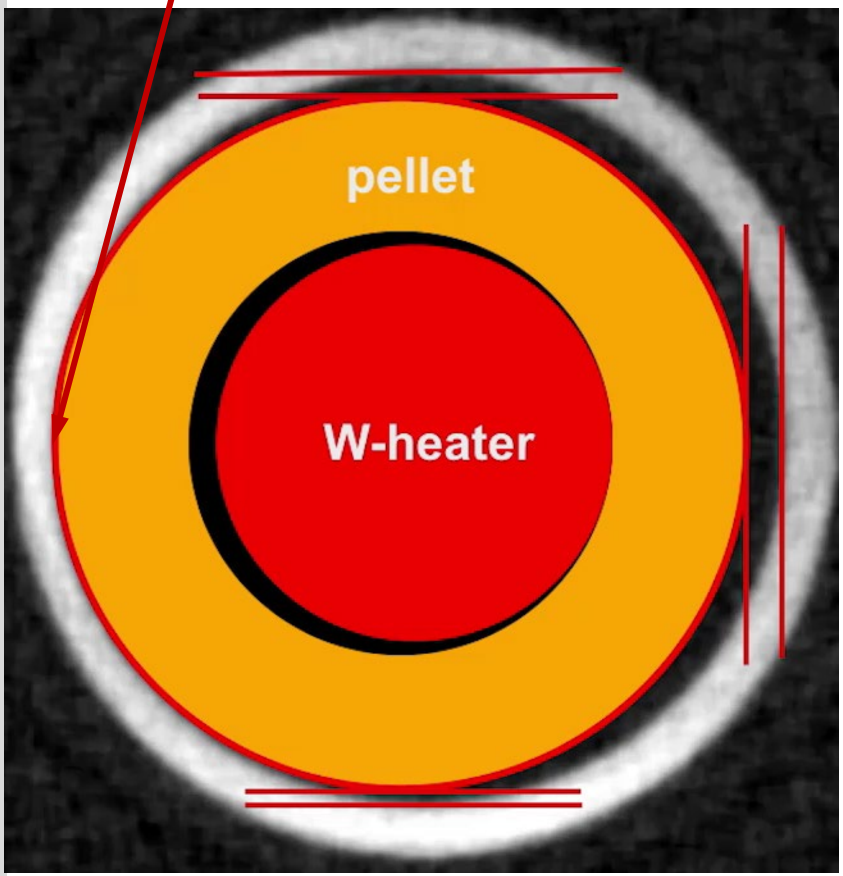

903 mm

Link to movie:

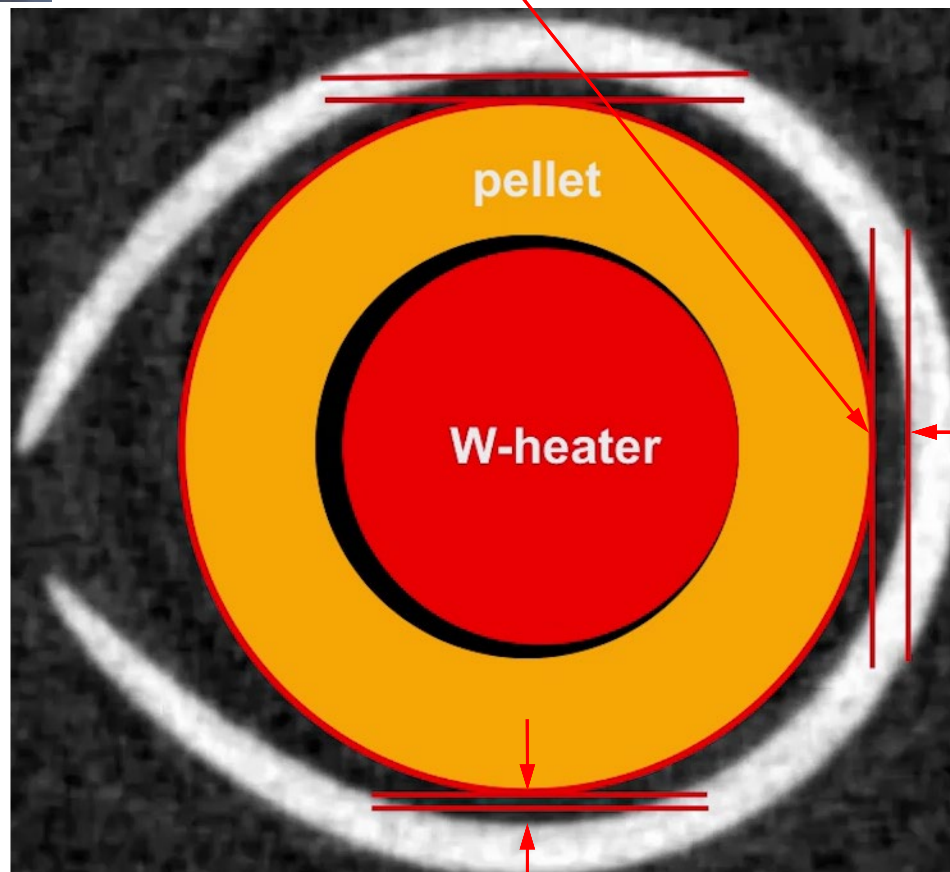

920 mm

gap increased during ballooning

REBEKA burst criterion (*burst strain* vs. *circumferential ΔT*) and FR2 in-pile test data

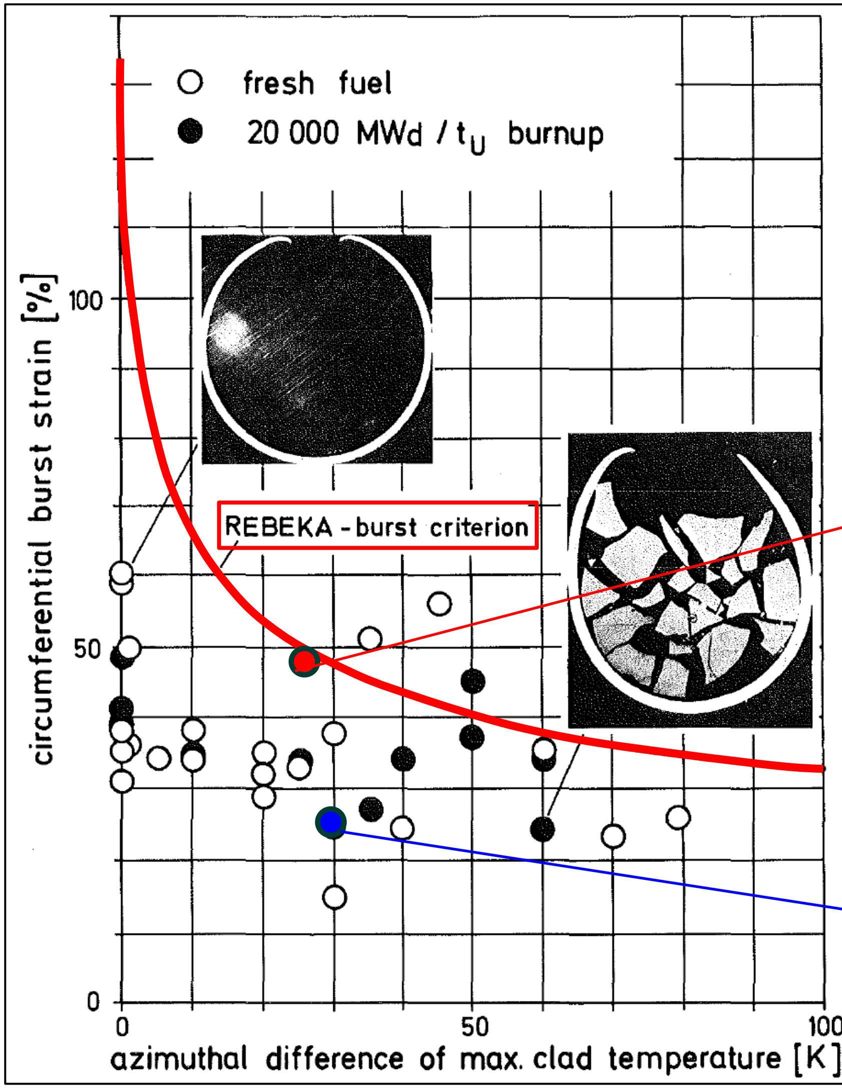

comparison of FR2 data with REBEKA burst criterium

The circumferential burst strains of cladding tubes are kept relatively small due to *temperature differences* on the cladding circumference and the anisotropic strain behavior of Zr alloys.

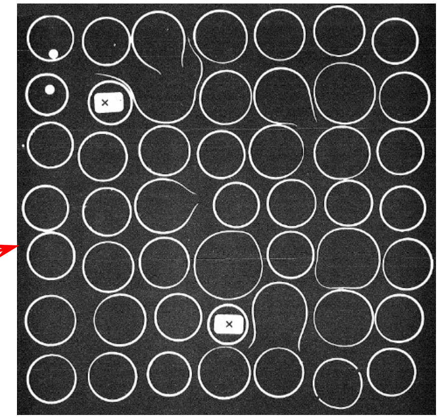

REBEKA-5 bundle at 2000 mm with maximum bundle blockage of 52%: maximum clad strain **49%**

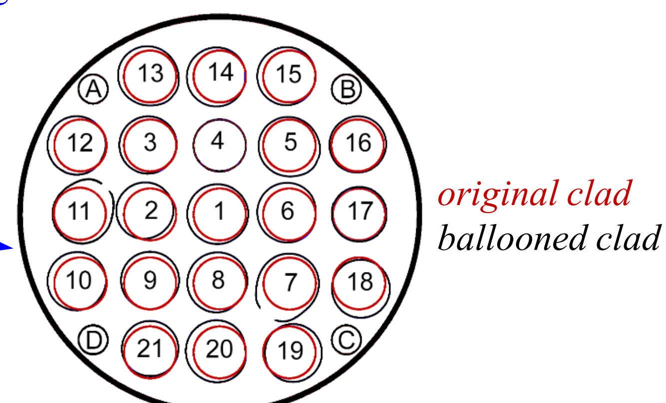

QUENCH-LOCA-4 bundle at 924 mm with maximum bundle blockage of 19%: maximum clad strain **23%**

Cladding deformation under circumferential temperature gradient

- Up to burnups of 30 MWd/kgU, fuel pellets can only have point contact with the cladding (and not along their entire perimeter), which leads to a hot spot in this place.

- The cladding begins to unsymmetrical stretch in directions perpendicular to the tangent line of contact between the pellet and the cladding, and then ruptures near the contact point with additional outward deformation of the burst opening edges.

- The circumferential strains of the claddings are generally no more than 40%, which leads to maximum blockades of the bundle cross-section of about 60%, which in turn ensures full coolability of the bundle during reflood.

Acknowledgment

The author would like to thank the entire QUENCH team for their intensive work during the test preparations and post-test investigations.

Thank you for your attention

https://www.iam.kit.edu/awp/english/163.php

http://quench.forschung.kit.edu/